Nano Research
2022, 15(4): 3775–3780

ISSN 1998-0124 CN 11-5974/O4
https://doi.org/10.1007/s12274-021-3922-x

Research Article

The role of Cu crystallographic orientations towards growing superclean graphene on meter-sized scale

Xiaoting Liu[1,2,3,§], Jincan Zhang[1,2,3,4,§], Wendong Wang[5,§], Wei Zhao[6,§], Heng Chen[1,3], Bingyao Liu[1,2,3,7], Mengqi Zhang[3], Fushun Liang[1,3], Lijuan Zhang[3], Rui Zhang[5], Ning Li[3], Yuexin Zhang[3], Yuchen Liu[3], Kaicheng Jia[1,3], Luzhao Sun[1,2,3], Yixuan Zhao[1,3], Peng Gao[1,2,3,7], Qinghong Yuan[6,8], Li Lin[1,3,5,9] (✉), Hailin Peng[1,2,3] (✉), and Zhongfan Liu[1,2,3] (✉)

[1] *Center for Nanochemistry, Beijing Science and Engineering Center for Nanocarbons, Beijing National Laboratory for Molecular Science, College of Chemistry and Molecular Engineering, Peking University, Beijing 100871, China*
[2] *Academy for Advanced Interdisciplinary Studies, Peking University, Beijing 100871, China*
[3] *Beijing Graphene Institute, Beijing 100095, China*
[4] *Department of Engineering, University of Cambridge, Cambridge, CB3 0FA, UK*
[5] *School of Physics and Astronomy, University of Manchester, Manchester, M13 9PL, UK*
[6] *State Key Laboratory of Precision Spectroscopy, School of Physics and Electronic Science, East China Normal University, Shanghai 200241, China*
[7] *Electron Microscopy Laboratory and International Center for Quantum Materials, School of Physics, Peking University, Beijing 100871, China*
[8] *Centre for Theoretical and Computational Molecular Science, Australian Institute for Bioengineering and Nanotechnology, The University of Queensland, Brisbane, QLD 4072, Australia*
[9] *School of Materials Science and Engineering, Peking University, Beijing 100871, China*
[§] *Xiaoting Liu, Jincan Zhang, Wendong Wang, and Wei Zhao contributed equally to this work.*

Received: 28 July 2021 / **Revised:** 17 September 2021 / **Accepted:** 30 September 2021

ABSTRACT

Chemical vapor deposition (CVD)-grown graphene films on Cu foils, exhibiting fine scalability and high quality, are still suffering from the adverse impact of surface contamination, i.e., amorphous carbon. Despite the recent successful preparation of superclean graphene through Cu-vapor-assisted reactions, the formation mechanism of amorphous carbon remains unclear, especially with regard to the functions of substrates. Herein, we have found that the crystallographic orientations of underlying metal substrates would determine the cleanness of graphene in such a way that slower diffusion of active carbon species on as-formed graphene-Cu(100) surface is the key factor that suppresses the formation of contamination. The facile synthesis of clean graphene is achieved on the meter-sized Cu(100) that is transformed from the polycrystalline Cu foils. Furthermore, a clean surface of graphene on Cu(100) ensures the reduction of transfer-related polymer residues, and enhanced optical and electrical performance, which allows for versatile applications of graphene in biosensors, functioning as flexible transparent electrodes. This work would offer a promising material platform for the fundamental investigation and create new opportunities for the advanced applications of high-quality graphene films.

KEYWORDS

superclean graphene, Cu crystallographic orientations, Cu(100) foil, improved electrical performance

1 Introduction

Chemical vapor deposition (CVD) growth of graphene on metal substrates, especially on commercially available Cu foils, exhibits remarkable scalability and quality, and has attracted tremendous attention from researchers and industries in recent years [1–5]. However, the surface contamination on graphene surface has been widely reported to strongly degrade the promising properties of CVD graphene [6–9], and impede its applications, where a clean surface is especially needed [10–12]. Recently, the origin of the surface contamination has been found to be rooted in the process of high-temperature CVD growth, where the intrinsic contamination, i.e., amorphous carbon, is produced on graphene surface due to the insufficient supply of Cu catalysis [13–16]. Despite recent efforts to grow clean graphene by suppressing the formation of amorphous carbon during the growth [13, 14] or the removal of the contamination by post-treatment [15, 16], the formation mechanism of amorphous carbon, especially the functions of underlying substrates, is still unclear.

Cu foils are the widely used growth substrates for the growth of high-quality graphene films because of the better control over the thickness and domain size [17–19]. However, commercially available Cu foils are usually composed of domains with different crystallographic orientations, delivering a polycrystalline nature of Cu foils. Distinct growth behaviors of graphene were observed on different Cu surfaces [20–24], in terms of symmetry and shape of graphene domains, which are caused by the different catalytic abilities of Cu surface, primarily owing to the distinct configuration of metal atoms. Such catalytic ability of Cu surface governs the elementary steps of the graphene growth, including the decomposition of carbon source, adsorption,

Address correspondence to Li Lin, linli-cnc@pku.edu.cn; Hailin Peng, hlpeng@pku.edu.cn; Zhongfan Liu, zfliu@pku.edu.cn

diffusion and desorption of carbon species and the nucleation of graphene [25–28].

Herein, we find the crystallographic orientations of Cu foils are vital for the formation of amorphous carbon on graphene surface, and, in particular, the surface of graphene grown on Cu(100) (G-Cu(100)) is cleaner than those grown on other Cu surfaces. The suppressed formation of amorphous carbon is ascribed to the slow diffusion of carbon species on G-Cu(100) surface, which is confirmed by density functional theory (DFT) calculation. After mass production of meter-sized Cu(100) with the assistance of oxygen, the large-area growth of clean graphene films is achieved. Meanwhile, the clean graphene surface enables the reduction of polymer residues after the transfer of graphene onto functional substrates. The clean graphene with enhanced optical and electrical performances is employed as flexible transparent electrodes for versatile applications in biosensors. The large-area growth of clean graphene creates new opportunities for fundamental exploration and application development in the near future.

2 Results and discussion

After the graphene growth, we transferred graphene onto transmission electron microscopy (TEM) grids without using the polymer, which would allow us to readily observe the amorphous carbon [29]. The amorphous carbon contamination on graphene surface displays a darker contrast than graphene in a TEM image. The size of continuous clean graphene regions is around tens of nanometers, with an areal ratio of clean regions (cleanness) less than 50% (Fig. 1(a) and Figs. S1–S3 in the Electronic Supplementary Material (ESM)). Such surface contamination was reported to be originated from high-temperature CVD growth [13]. In combination of *in situ* transfer method, we investigated the correspondence between crystallographic orientations of underlying Cu and graphene cleanness, in which five typical Cu crystallographic orientations were used for comparison (Fig. 1(b), and Figs. S4 and S5 in the ESM). Note that the crystallographic orientations of polycrystalline Cu foil were probed by using the electron backscatter diffraction (EBSD) measurement (inset of Fig. 1(c)). Interestingly, the cleanness of G-Cu(100) is higher than that of the graphene grown on other four types of Cu surfaces (Fig. 1(b) and Figs. S6–S8 in the ESM), which implies that less amorphous carbon is formed on the surface of G-Cu(100). Thus, the surface cleanness of CVD-grown graphene is highly related to the Cu crystallographic orientations (Fig. 1(c)).

DFT calculation was conducted to probe the formation mechanism of amorphous carbon on graphene/Cu surfaces (Fig. S9 and Table S1 in the ESM), which would help understand the contribution of Cu crystallographic orientations to the formation of amorphous carbon. Formation of amorphous carbon contamination should include three steps: (1) production of active carbon species in the gas phase and on Cu substrate; (2) nucleation of amorphous carbon on graphene surface; (3) growth of amorphous carbon contamination on graphene surface. Note that, the formation of amorphous carbon and growth of graphene occur at the same time, but at different locations [30]. The fundamental picture of amorphous carbon formation should be as follows: After the production of active carbon species that is CH in the case of growth of graphene on Cu [26], the fast diffusion of CH species on graphene surface and collision among the moving carbon species would result in the nucleation of amorphous carbon on graphene surface. Note that, the desorption rate of CH species from graphene surface is much smaller than its diffusion rate (Fig. S10 in the ESM); therefore, the diffusion process is the dominating step in the formation of amorphous carbon contamination on graphene surface. The dendritic shaped structure of amorphous carbon also indicates the diffusion-limited growth of amorphous carbon on graphene surface (Fig. S11 in the ESM), referring to the growth dynamic of graphene on Cu surface [31]. Therefore, the slow diffusion of active carbon species on surface of G-Cu(100) would inhibit the formation of amorphous carbon on graphene (Figs. 1(d) and 1(e)). In detail, according to the DFT calculation, the diffusion barrier of CH species on G-Cu(100) (1.18 eV) is higher than that of CH species moving on other four types of Cu crystallographic orientations (Fig. 1(f)), confirming that the diffusion rate of CH species on Cu(100) is

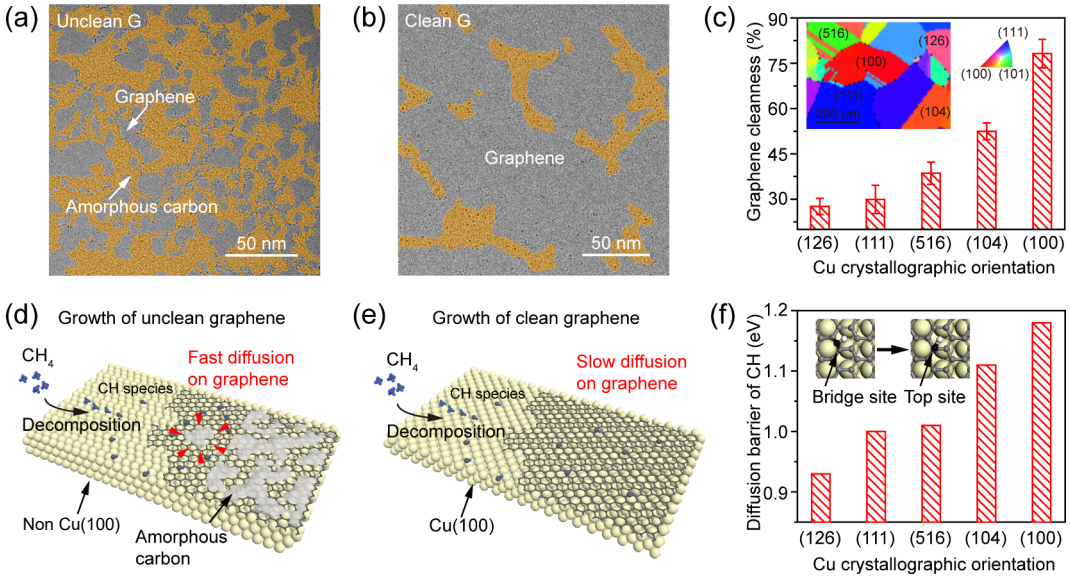

Figure 1 Growth of clean graphene on Cu(100). (a) and (b) TEM images of unclean graphene (a) with the obvious distribution of amorphous carbon and clean graphene (b). (c) Comparison of the cleanness of graphene films grown on polycrystalline Cu foils. Inset: EBSD mapping of graphene grown on polycrystalline Cu substrate. (d) and (e) Schematic diagrams of the growth of graphene on Cu(100) (e) and on other Cu surfaces (d) with different crystallographic orientations. The fast diffusion of CH species on graphene surface would result in the nucleation and growth of amorphous carbon (grey), while the slow diffusion of CH species on G-Cu(100) would suppress the formation of amorphous carbon. (f) The relationship of the diffusion barriers of CH species on G-Cu with the different crystallographic orientations of Cu. Inset: The diffusion of CH species on G-Cu surface from bridge site to top site, based on which process the diffusion barriers of CH species were calculated.

much slower. Thus, the nucleation of amorphous carbon would be suppressed on G-Cu(100) surface, ensuring a cleaner surface. Moreover, the calculation results of diffusion barriers of CH on graphene on corresponding five Cu crystallographic orientations agree well with the observed cleanness in Fig. 1(c), further indicating the correspondence between diffusion barriers of CH species and the formation of amorphous carbon. This understanding of formation mechanism of amorphous carbon should be instructive for the preparation of ideal metal substrates for growing superclean graphene.

Figure 2(a) illustrates the schematic of the batch-to-batch production of clean graphene films grown on large-area Cu(100) foils, in which the oxygen was introduced to initiate the transformation of polycrystalline Cu foils into Cu(100). Specifically, the oxygen chemisorbed on Cu surface could stabilize the Cu(100) orientation and impede the evolution of other Cu crystallographic orientations [32, 33]. With the assistance of oxygen, large-area Cu(100) (0.6 m × 0.1 m) substrates were successfully prepared (Fig. 2(b)), whose crystallographic orientation was confirmed by X-ray diffraction (XRD) patterns (Fig. 2(c) and Fig. S12 in the ESM), EBSD results (Fig. 2(d) and Fig. S13 in the ESM), and atomic force microscopy (AFM) images (Fig. S14 in the ESM).

The growth of square-shaped graphene single crystals and continuous films on as-received Cu (100) was then achieved (Figs. 2(e)–2(g)), in which 15 min is sufficient for the full coverage of graphene on Cu surface. The improved cleanness of the nine meter-sized pieces of samples was further confirmed by the statistical results (Figs. 2(h) and 2(i)). In addition, the high-resolution TEM (HRTEM) displays a perfect hexagonal graphene lattice (inset of Fig. 2(h)). Noise-level D band intensity in the Raman spectra also proves the high quality of graphene films (Fig. S15 in the ESM), implying the great advantages of clean graphene in numerous applications, especially for those that require clean, flat surface/interface, such as TEM imaging.

The inevitable transfer of graphene grown on metal is another process that would introduce contamination, and the amount of polymer residues is also related to the cleanness of CVD-grown graphene surface [13–16]. In this regard, white light interferometry (WLI) is sensitive to the surface topography, and is capable of fast evaluation of surface topography on a large scale [34]. To get a clear comparison of graphene cleanness, WLI was used to probe the surface roughness of continuous graphene grown on a region composed of both Cu(100) and Cu(111) domains after the transfer onto atomically flat mica substrate (Fig. S16 in the ESM). The surface contamination on G-Cu(111) displays a higher height than the surface of as-transferred G-Cu(100), confirming the reduction of polymer residues on G-Cu(100) after the transfer.

The reduced surface contamination also contributes to the improved electrical properties of as-received clean graphene, such as the electrical conductivity which would contribute to achieve improved performance of graphene-based devices, such as organic light-emitting diodes (OLEDs), and solar cells [11, 35]. The as-received clean G-Cu(100) exhibits improved electrical conductivity with an average sheet resistance value of 248.7 ± 43.7 $\Omega \cdot sq^{-1}$, which is much lower than that of its unclean counterpart (419.5 ± 94.6 $\Omega \cdot sq^{-1}$) (Fig. 3(a)). Note that the large-scale evaluation of sheet resistance is conducted by a macroscopic four-probe method, and the detected region for measuring the conductivity is mm-sized (inset of Fig. 3(a) and Fig. 3(b)). Clean graphene films after transfer to quartz substrates also show a high light transmittance, which is comparable to the theoretical simulation results [36] (Fig. S17 in the ESM). Meanwhile, the improved light transmittance of clean graphene is also verified by contrast spectrum measurement (Fig. S18 in the ESM). Moreover, graphene was transferred onto the polymer substrates, and was employed as flexible transparent electrodes for monitoring the bioelectrical signals, including electrooculogram (EOG), electrocardiogram (ECG) and electromyogram (EMG) (Fig. 3(c)). Specifically, when the volunteer moved his eyes right and left, EOG signals were measured with an opposite amplitude (Fig. 3(d)). Graphene electrodes were placed onto the left and right forearms of the volunteer to monitor ECG signals (Fig. 3(e)). When the volunteer squeezed the handgrip at a different degree, EMG signals with different amplitudes can be monitored accordingly (Fig. 3(f)). These sensors allow the real-time detection of high-quality bioelectrical signals with a broad sensing range, low limit detection and high sensitivity.

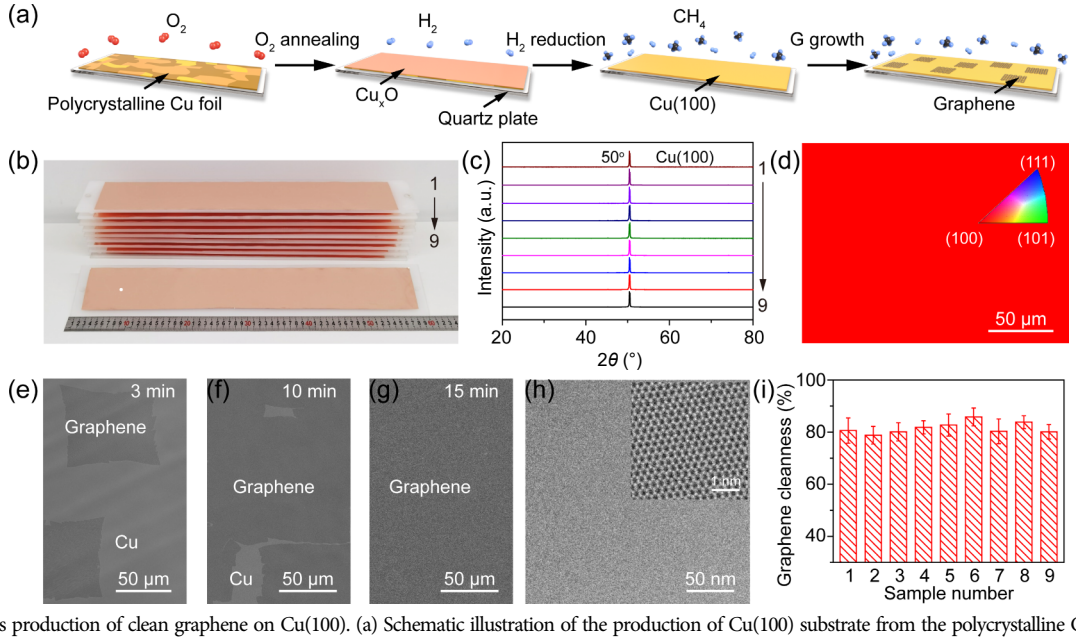

Figure 2 Mass production of clean graphene on Cu(100). (a) Schematic illustration of the production of Cu(100) substrate from the polycrystalline Cu foil, and the subsequent growth of graphene domains on Cu(100) on large scale. (b) Photograph of ten pieces of large-area graphene films grown on Cu(100) substrates. (c) Representative XRD patterns collected in the as-received large-area Cu(100) films from vertical top (1) to bottom (9) as marked in (b). (d) Representative EBSD image of as-received Cu(100) substrate. (e)–(g) SEM images of graphene grown on Cu(100) with the growth time of (e) 3, (f) 10 and (g) 15 min. (h) TEM image of clean graphene grown on Cu(100). Inset: HRTEM image of clean graphene film. (i) Statistics of cleanness for clean graphene grown on the nine pieces of Cu(100) substrates.

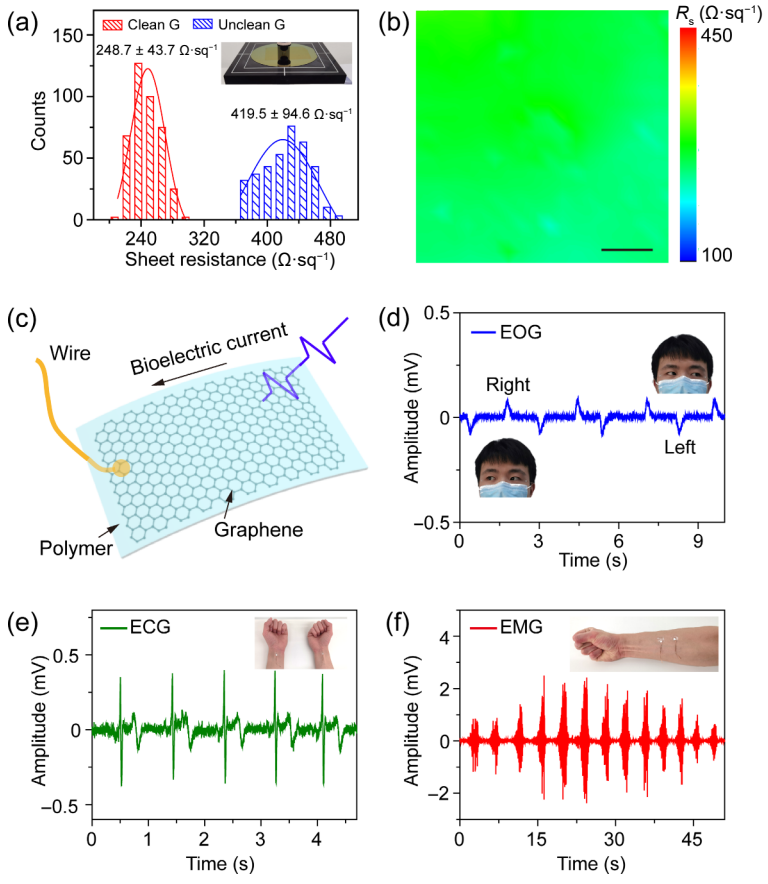

Figure 3 Electrical properties and electrophysiological performance of clean G-Cu(100). (a) Statistics of sheet resistance of G-Cu(100) (red) and unclean graphene (blue). Inset: photograph of the facility for the large-scale measurement of sheet resistance by a macroscopic four-probe method. (b) Sheet resistance mapping of G-Cu(100) transferred onto SiO_2/Si substrate. The scale bar is 2 mm. (c) Schematic illustration of the function of graphene electrodes for recording the bioelectrical signals. (d) Electrooculogram sensing around eyes with graphene electrodes to monitor the horizontal eye electricity. Inset: photographs of eyes of volunteer moved right and left. (e) Characteristic signals of electrocardiogram. Inset: photograph of the measuring electrodes placed onto the left and right forearms of the volunteer. (f) The electrical activity of forearm when the volunteer squeezed the handgrip at different degrees. Inset: photograph of the measuring electrodes placed onto the forearm of the volunteer.

To further investigate the electrical properties of the clean graphene, we carefully measured its carrier mobility, by fabricating corresponding Hall bar devices of as-transferred graphene encapsulated by hBN [37]. The carrier mobility of the encapsulated clean graphene would reach 71,000 $cm^2 \cdot V^{-1} \cdot s^{-1}$ at room temperature (Fig. 4(a)) and 270,000 $cm^2 \cdot V^{-1} \cdot s^{-1}$ at 2.2 K (Fig. 4(b)), higher than the previous measurement results [38], confirming the improved electrical performance. Furthermore, the Shubnikov-de Haas (SdH) oscillations in longitudinal resistivity (R_{xx}) were observed at 2.2 K (Fig. 4(c)). Besides, low-temperature

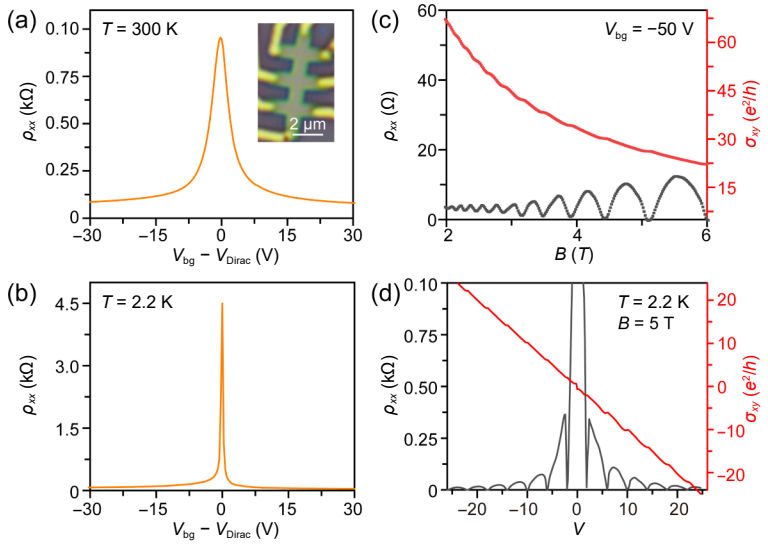

Figure 4 Transport characteristics of clean G-Cu(100). (a) Longitudinal resistivity of G-Cu(100) based device as a function of gate bias at 300 K. Inset: optical microscopy image of the as-fabricated Hall bar device. (b) Longitudinal resistivity of G-Cu(100) as a function of gate bias at 2.2 K. (c) Longitudinal resistivity (black) and Hall conductivity (red) as a function of magnetic field *B*. (d) Magnetoresistance (black) and Hall conductance (red) as a function of the Landau level filling factors of the quantum Hall states at low magnetic field of 5 T and temperature of 2.2 K.

magneto-transport measurements also exhibit a well-developed plateaus at quantized filling factors (ν), ±2, ±6, ±10, … (Fig. 4(d)). All above observation confirms the improved electrical properties of clean graphene, highlighting the advantages of growing clean graphene in the applications of future electronics.

3 Conclusion

In conclusion, we have demonstrated that Cu(100) substrate is the suitable substrate to grow high-quality, clean graphene films, and that the slower diffusion of CH active species on G-Cu(100) is responsible for the suppressed formation of amorphous carbon. For the mass production of clean graphene films, meter-sized clean graphene films were successfully synthesized on large-area Cu(100) substrates. Besides, the high cleanness of G-Cu(100) maintains after the transfer, which ensures the improved electrical performances and optical properties. Furthermore, the graphene electrodes can be used in the application of biosensors to acquire high-quality bioelectrical signals in real time. Our results provide a new insight into the formation mechanism of surface contamination on graphene and pave a new avenue to the industrial production of high-quality and clean graphene films for the future commercial applications, in which clean graphene surface is highly needed, such as TEM supporting membrane and epitaxial growth substrates for LEDs.

Acknowledgements

The authors thank Beijing National Laboratory for Molecular Science. This work was supported by Beijing National Laboratory for Molecular Sciences (No. BNLMS-CXTD-202001). This work was financially supported by the Beijing Municipal Science & Technology Commission (Nos. Z181100004818001 and Z201100008720005), the National Basic Research Program of China (No. 2016YFA0200101), and the National Natural Science Foundation of China (No. 52072042).

Electronic Supplementary Material: Supplementary material (further details of experiment, TEM measurements and so on) is available in the online version of this article at https://doi.org/10.1007/s12274-021-3922-x.

References

[1] Novoselov, K. S.; Fal′ko, V. I.; Colombo, L.; Gellert, P. R.; Schwab, M. G.; Kim, K. A roadmap for graphene. *Nature* **2012**, *490*, 192–200.

[2] Lin, L.; Peng, H. L.; Liu, Z. F. Synthesis challenges for graphene industry. *Nat. Mater.* **2019**, *18*, 520–524.

[3] Liu, C.; Wang, L.; Qi, J. J.; Liu, K. H. Designed growth of large-size 2D single crystals. *Adv. Mater.* **2020**, *32*, 2000046.

[4] Kong, W.; Kum, H.; Bae, S. H.; Shim, J.; Kim, H.; Kong, L. P.; Meng, Y.; Wang, K. J.; Kim, C.; Kim, J. Path towards graphene commercialization from lab to market. *Nat. Nanotechnol.* **2019**, *14*, 927–938.

[5] Pulizzi, F.; Bubnova, O.; Milana, S.; Schilter, D.; Abergel, D.; Moscatelli, A. Graphene in the making. *Nat. Nanotechnol.* **2019**, *14*, 914–918.

[6] Leong, W. S.; Wang, H. Z.; Yeo, J. J.; Martin-Martinez, F. J.; Zubair, A.; Shen, P. C.; Mao, Y. W.; Palacios, T.; Buehler, M. J.; Hong, J. Y. et al. Paraffin-enabled graphene transfer. *Nat. Commun.* **2019**, *10*, 867.

[7] Li, Z. T.; Wang, Y. J.; Kozbial, A.; Shenoy, G.; Zhou, F.; McGinley, R.; Ireland, P.; Morganstein, B.; Kunkel, A.; Surwade, S. P. et al. Effect of airborne contaminants on the wettability of supported graphene and graphite. *Nat. Mater.* **2013**, *12*, 925–931.

[8] Jia, Y. H.; Gong, X.; Peng, P.; Wang, Z. D.; Tian, Z. Z.; Ren, L. M.; Fu, Y. Y.; Zhang, H. Toward high carrier mobility and low contact resistance: Laser cleaning of PMMA residues on graphene surfaces. *Nano-Micro Lett.* **2016**, *8*, 336–346.

[9] Pettes, M. T.; Jo, I.; Yao, Z.; Shi, L. Influence of polymeric residue on the thermal conductivity of suspended bilayer graphene. *Nano Lett.* **2011**, *11*, 1195–1200.

[10] Kim, Y.; Cruz, S. S.; Lee, K.; Alawode, B. O.; Choi, C.; Song, Y.; Johnson, J. M.; Heidelberger, C.; Kong, W.; Choi, S. et al. Remote epitaxy through graphene enables two-dimensional material-based layer transfer. *Nature* **2017**, *544*, 340–343.

[11] Zhang, Z. K.; Du, J. H.; Zhang, D. D.; Sun, H. D.; Yin, L. C.; Ma, L. P.; Chen, J. S.; Ma, D. G.; Cheng, H. M.; Ren, W. C. Rosin-enabled ultraclean and damage-free transfer of graphene for large-area flexible organic light-emitting diodes. *Nat. Commun.* **2017**, *8*, 14560.

[12] Hong, H.; Zhang, J. C.; Zhang, J.; Qiao, R. X.; Yao, F. R.; Cheng, Y.; Wu, C. C.; Lin, L.; Jia, K. C.; Zhao, Y. C. et al. Ultrafast broadband charge collection from clean graphene/$CH_3NH_3PbI_3$ interface. *J. Am. Chem. Soc.* **2018**, *140*, 14952–14957.

[13] Lin L.; Zhang J. C.; Su H. S.; Li J. Y.; Sun L. Z.; Wang Z. H.; Xu F.; Liu C.; Lopatin S.; Zhu Y. H. et al. Towards super-clean graphene. *Nat. Commun.* **2019**, *10*, 1912.

[14] Jia, K. C.; Zhang, J. C.; Lin, L.; Li, Z. Z.; Gao, J.; Sun, L. Z.; Xue, R. W.; Li, J. Y.; Kang, N.; Luo, Z. T. et al. Copper-containing carbon feedstock for growing superclean graphene. *J. Am. Chem. Soc.* **2019**, *141*, 7670–7674.

[15] Zhang, J. C.; Jia, K. C.; Lin, L.; Zhao, W.; Quang, H. T.; Sun, L. Z.; Li, T. R.; Li, Z. Z.; Liu, X. T.; Zheng, L. M. et al. Large-area synthesis of superclean graphene via selective etching of amorphous carbon with carbon dioxide. *Angew. Chem., Int. Ed.* **2019**, *58*, 14446–14451.

[16] Sun, L. Z.; Lin, L.; Wang, Z. H.; Rui, D. R.; Yu, Z. W.; Zhang, J. C.; Li, Y. L. Z.; Liu, X. T.; Jia, K. C.; Wang, K. X. et al. A force-engineered lint roller for superclean graphene. *Adv. Mater.* **2019**, *31*, 1902978.

[17] Mattevi, C.; Kim, H.; Chhowalla, M. A review of chemical vapour deposition of graphene on copper. *J. Mater. Chem.* **2011**, *21*, 3324–3334.

[18] Hao, Y. F.; Bharathi, M. S.; Wang, L.; Liu, Y. Y.; Chen, H.; Nie, S.; Wang, X. H.; Chou, H.; Tan, C.; Fallahazad, B. et al. The role of surface oxygen in the growth of large single-crystal graphene on copper. *Science* **2013**, *342*, 720–723.

[19] Zhou, H. L.; Yu, W. J.; Liu, L. X.; Cheng, R.; Chen, Y.; Huang, X. Q.; Liu, Y.; Wang, Y.; Huang, Y.; Duan, X. F. Chemical vapour deposition growth of large single crystals of monolayer and bilayer graphene. *Nat. Commun.* **2013**, *4*, 2096.

[20] Wood, J. D.; Schmucker, S. W.; Lyons, A. S.; Pop, E.; Lyding, J. W. Effects of polycrystalline Cu substrate on graphene growth by chemical vapor deposition. *Nano Lett.* **2011**, *11*, 4547–4554.

[21] Li, B. W.; Luo, D.; Zhu, L. Y.; Zhang, X.; Jin, S.; Huang, M.; Ding, F.; Ruoff, R. S. Orientation-dependent strain relaxation and chemical functionalization of graphene on a Cu (111) foil. *Adv. Mater.* **2018**, *30*, 1706504.

[22] Artyukhov, V. I.; Hao, Y. F.; Ruoff, R. S.; Yakobson, B. I. Breaking of symmetry in graphene growth on metal substrates. *Phys. Rev. Lett.* **2015**, *114*, 115502.

[23] Xia, K. L.; Artyukhov, V. I.; Sun, L. F.; Zheng, J. Y.; Jiao, L. Y.; Yakobson, B. I.; Zhang, Y. Y. Growth of large-area aligned pentagonal graphene domains on high-index copper surfaces. *Nano Res.* **2016**, *9*, 2182–2189.

[24] Murdock, A. T.; Koos, A.; Ben Britton, T.; Houben, L.; Batten, T.; Zhang, T.; Wilkinson, A. J.; Dunin-Borkowski, R. E.; Lekka, C. E.; Grobert, N. Controlling the orientation, edge geometry, and thickness of chemical vapor deposition graphene. *ACS Nano* **2013**, *7*, 1351–1359.

[25] Shu, H. B.; Tao, X. M.; Ding, F. What are the active carbon species during graphene chemical vapor deposition growth. *Nanoscale* **2015**, *7*, 1627–1634.

[26] Wang, X. L.; Yuan, Q. H.; Li, J.; Ding, F. The transition metal surface dependent methane decomposition in graphene chemical vapor deposition growth. *Nanoscale* **2017**, *9*, 11584–11589.

[27] Zhang, W. H.; Wu, P.; Li, Z. Y.; Yang, J. L. First-principles

thermodynamics of graphene growth on Cu surfaces. *J. Phys. Chem. C* **2011**, *115*, 17782–17787.

[28] Wu, P.; Zhang, W. H.; Li, Z. Y.; Yang, J. L. Mechanisms of graphene growth on metal surfaces: Theoretical perspectives. *Small* **2014**, *10*, 2136–2150.

[29] Zhang, J. C.; Lin, L.; Sun, L. Z.; Huang, Y. C.; Koh, A. L.; Dang, W. H.; Yin, J. B.; Wang, M. Z.; Tan, C. W.; Li, T. R. et al. Clean Transfer of large graphene single crystals for high-intactness suspended membranes and liquid cells. *Adv. Mater.* **2017**, *29*, 1700639.

[30] Zhang, J. C.; Sun, L. Z.; Jia, K. C.; Liu, X. T.; Cheng, T.; Peng, H. L.; Lin, L.; Liu, Z. F. New growth frontier: Superclean graphene. *ACS Nano* **2020**, *14*, 10796–10803.

[31] Dong, J. C.; Zhang, L. N.; Ding, F. Kinetics of graphene and 2D materials growth. *Adv. Mater.* **2019**, *31*, 1801583.

[32] Wang, H.; Xu, X. Z.; Li, J. Y.; Lin, L.; Sun, L. Z.; Sun, X.; Zhao, S. L.; Tan, C. W.; Chen, C.; Dang, W. H. et al. Surface monocrystallization of copper foil for fast growth of large single-crystal graphene under free molecular flow. *Adv. Mater.* **2016**, *28*, 8968–8974.

[33] Hu, J. X.; Xu, J. B.; Zhao, Y. F.; Shi, L.; Li, Q.; Liu, F. K.; Ullah, Z.; Li, W. W.; Guo, Y. F.; Liu, L. W. Roles of oxygen and hydrogen in crystal orientation transition of copper foils for high-quality graphene growth. *Sci. Rep.* **2017**, *7*, 45358.

[34] Deck, L.; De Groot, P. High-speed noncontact profiler based on scanning white-light interferometry. *Appl. Opt.* **1994**, *33*, 7334–7338.

[35] Loh, K. P.; Tong, S. W.; Wu, J. S. Graphene and graphene-like molecules: Prospects in solar cells. *J. Am. Chem. Soc.* **2016**, *138*, 1095–1102.

[36] Nair, R. R.; Blake, P.; Grigorenko, A. N.; Novoselov, K. S.; Booth, T. J.; Stauber, T.; Peres, N. M. R.; Geim, A. K. Fine structure constant defines visual transparency of graphene. *Science* **2008**, *320*, 1308.

[37] Kim, K.; Yankowitz, M.; Fallahazad, B.; Kang, S.; Movva, H. C. P.; Huang, S. Q.; Larentis, S.; Corbet, C. M.; Taniguchi, T.; Watanabe, K. et al. Van der Waals heterostructures with high accuracy rotational alignment. *Nano Lett.* **2016**, *16*, 1989–1995.

[38] De Fazio, D.; Purdie, D. G.; Ott, A. K.; Braeuninger-Weimer, P.; Khodkov, T.; Goossens, S.; Taniguchi, T.; Watanabe, K.; Livreri, P.; Koppens, F. H. L. et al. High-mobility, wet-transferred graphene grown by chemical vapor deposition. *ACS Nano* **2019**, *13*, 8926–8935.